TEM and EELS measurements of interface roughness in epitaxial Fe/MgO/Fe magnetic tunnel junctions

V. Serin,[1,][*] S. Andrieu,[2] R. Serra,[1] F. Bonell,[2] C. Tiusan,[2] L. Calmels,[1] M. Varela,[3] S. J. Pennycook,[3] E. Snoeck,[1] M. Walls,[4] and C. Colliex[4]

[1]*CEMES-CNRS, BP 4347, 31055 Toulouse, France*

[2]*LPM, CNRS/Nancy Université, UMR7556, BP 239, F-54506 Vandoeuvre, France*

[3]*Materials Science and Technology Division, Oak Ridge National Laboratory, Oak Ridge, Tennessee 37831, USA*

[4]*Laboratoire de Physique des Solides (CNRS UMR 8502), Université Paris Sud 11, F-91405 Orsay, France*

The crystalline structure, chemical composition, and bonding states across epitaxial Fe/MgO/Fe(001) magnetic tunnel junctions grown by molecular-beam epitaxy have been investigated down to the atomic scale by spatially resolved electron energy-loss spectroscopy. Both metal-insulator interfaces exhibit significant roughness, which can be attributed to Fe and MgO terraces overlapping one another. These terraces extend over typical widths of 6–10 nm parallel to the interface and over typical heights below 1 nm, and a structural asymmetry of the roughness is revealed. These features could be responsible for the nonsymmetrical transport properties measured when reversing the applied voltage.

PACS number(s): 79.20.Uv, 68.37.Lp, 85.75.−d, 73.40.Rw

I. INTRODUCTION

Magnetic tunnel junctions (MTJs) have been widely studied over the past few years due to their great potential application in spintronic devices such as sensors or nonvolatile magnetic random access memories.[1,2] In these junctions, electrons travel by tunneling between two ferromagnetic layers separated by a thin insulating barrier and the tunnel resistance depends on the relative orientation of the magnetization of both electrodes. Most of the experimental and theoretical studies on MTJs have shown that the tunnel magnetoresistance (TMR) strongly depends on the atomic structure of the barrier and of the magnetic electrodes. This can clearly be seen from the comparison between polycrystalline and single-crystal MTJs: the tunnel magnetoresistance of the junctions which use a polycrystalline or an amorphous barrier[3–6] is indeed lowered by the low barrier height, the interface roughness, the difficulty to control the degree of oxidation throughout the amorphous insulating layer,[7] the magnetism of the polycrystalline ferromagnetic electrodes, and the complexity of the transport mechanisms across the disordered insulator. The situation is different for single-crystal oxide barriers grown in epitaxial orientation with respect to the magnetic films, for which recent calculations have predicted high TMR values. A TMR ratio of 1000% has for instance been predicted for an epitaxial Fe/MgO/Fe(001).[8,9] This high theoretical TMR has motivated experimental efforts for building single-crystal MTJs of very good structural quality. TMR ratios of 180%, 340%, and 420% have, respectively, been reported for single-crystal Fe/MgO/Fe(001) junctions at room temperature[10,11] and at 5 K,[12] and for Co/MgO/Co single-crystal MTJs at room temperature.[13] Large TMR values ranging between 220% (Ref. 14) and 500% (Ref. 15) have also been observed for CoFeB/MgO/CoFeB MTJs grown by sputtering and crystallized by annealing after growth. These exceptional transport properties are due to coherent tunneling mechanisms in which quantum correlation is preserved between the two sides of the barrier. Coherent tunneling only exists in high

quality epitaxial junctions and explains phenomena such as oscillations of the TMR as a function of the insulating barrier thickness,[10] quantum well effects in Fe/Cr/Fe/MgO/Fe MTJs,[16] or reduction of the magnetotransport due to minority-spin interfacial resonant states.[17–19]

The magnetotransport properties of a MTJ depend not only on the crystal structure of the barrier and magnetic electrodes, but also on the quality of the two interfaces of the junction. Calculations have for instance predicted that an interfacial iron oxide layer modifies the transport properties of Fe/MgO/Fe MTJs.[20] Usually, the conductance and the TMR measured in experiments are not even functions of the bias voltage.[10,18] The fact that the conductance differs when electrons are injected from one side or from the other side of the junction means that the atomic structure is different for the two interfaces. Previous studies have investigated the structural and chemical qualities of these interfaces.

The bottom interface, which results from the two-dimensional growth of MgO on Fe(001), is nearly perfect.[11,21–23] No Fe-O hybridization has been detected for one Fe flat atomic plane in contact with a very thin MgO(001) barrier by x-ray photoemission spectroscopy (XPS) or x-ray absorption experiments (XAS).[21,22,24] It has nevertheless been proposed to explain measurements by surface diffraction experiments performed on the Fe/MgO interface.[25] However, this is an indirect determination compared to photoemission or absorption measurements.

The second top interface, which results from the three-dimensional growth of Fe on the MgO barrier, is less flat: the critical thickness for plastic relaxation of MgO on Fe(001) is indeed rather small (between 4 and 5 atomic planes) (Ref. 23) and we used junctions with a MgO thickness of 2.5–3 nm in order to obtain a good spin filtering effect.[9] This means that the MgO barriers are relaxed in our samples and that the top MgO barrier surface is rougher than the first Fe/MgO interface. Such an increased roughness could lead to an enhanced Fe-O hybridization for Fe atoms located on steps or on threading dislocations. This assumption is supported by a previous study which concluded in a weak hy-

bridization for the top interface.[24] However, a rapid calculation using Fe and MgO surface energies and assuming a reasonable island density around 10^{11-12} cm^{-2} allows us to calculate that, in their experiments, only 10%–20% of the XPS signal comes from the interface of the top Fe islands with the MgO. The rest of signals are coming from the "bulk" Fe atoms belonging to the Fe islands on top of the interface. Therefore, due to this three-dimensional (3D) Fe growth on the MgO, the Fe-O hybridization at this second interface is difficult to detect and correctly interpret from XPS experiments.

The experimental techniques which have been used up to now to study the structure of the bottom and top interfaces have mainly given information averaged over large interface areas. Advanced techniques for atomic scale study of the structural, chemical, and electronic structures are therefore necessary for a refined analysis of the two interfaces of a MTJ. In this paper, we present a transmission electron microscopy (TEM) investigation of the Fe/MgO and MgO/Fe interfaces in epitaxial Fe/MgO/Fe magnetic tunnel junctions prepared by molecular-beam epitaxy (MBE). The local chemical composition and electronic structure have been investigated by electron energy-loss spectroscopy (EELS), a technique which has already been demonstrated to be efficient for local investigations of thin oxide films,[26–28] with a spatial resolution which can be as small as 0.1 nm. The recorded maps and profiles emphasize the presence of MgO and Fe terraces, with typical width and height being responsible for the observed roughness of the interfaces. Furthermore, fine structures of the oxygen K-edge spectrum have also been used to identify a local Fe-O hybridization. The differences between the atomic and electronic structures which have been measured at the two interfaces can be used to understand the asymmetry of the magnetotransport properties of the junction as a function of the direction of the applied voltages. Our paper is organized as follows. Section II describes sample preparation from the growth of the junctions to the thinning of transverse sections for TEM studies. Experimental results are reported in Sec. III, followed by a short description of the highlights of the present contribution within the general issue of understanding and controlling MTJ properties.

II. SAMPLE PREPARATION

The Fe/MgO/Fe stacks were grown in a MBE system on MgO(100) substrates. The growth conditions of single crystalline Fe films on MgO, and MgO barriers on Fe, have already been reported[29,30] and we only repeat here the most important of these conditions. The MgO substrates are bottom out-gassed *in situ* at 1200 K to eliminate the carbon contamination. A 10 nm thick MgO layer is subsequently epitaxially grown on the MgO substrate in order to trap residual carbon impurities.[11] The Fe first MTJ electrode is grown at room temperature in a vacuum which does not exceed 5.10^{-11} Torr. An annealing at 750 K leads to flat Fe surfaces free of oxygen and carbon, as checked by Auger-electron spectroscopy (AES) and XPS. The roughness and the terrace size of this first Fe layer have been investigated

using scanning tunneling microscopy (STM). The growth of the different layers has been controlled *in situ* by reflection high energy electron diffraction (RHEED). No interdiffusion between Fe and MgO was observed at room temperature, as checked by AES and XPS techniques, which also shows that the mixing between Fe and MgO only takes place at temperatures higher than 900 K, far above the temperatures which have been used during growth or surface smoothing in our standard samples.

In order to study and understand the structure of the two interfaces, TEM observations and EELS measurements were performed on three specific samples grown with the following stacking sequences:

Sample 1: MgO substrate//MgO 10 nm/Fe 42 nm/MgO 20 nm.

Sample 2: MgO substrate//MgO 10 nm/Fe 38 nm/MgO 10 nm/Fe 38 nm/MgO.

Sample 3: MgO substrate//MgO 10 nm/Fe 8 nm/MgO 1.5 nm/Fe 30 nm/Co 15 nm/MgO.

In all samples, the 10 nm width MgO underlayer grown on the substrate plays only the role of a residual carbon trapping layer. In the following, all comments about the MgO will only concern the insulating barrier of the MTJ deposited on top of the first Fe electrode. Sample 1, which only contains the first Fe electrode covered by a thick MgO barrier, has been grown to analyze the bottom Fe/MgO interface. The top MgO/Fe interface is investigated with sample 2, which contains a thick MgO barrier (10 nm) in order to efficiently separate the information coming from each interface. The barrier thickness in MTJs being much thinner than 10 nm, we have also grown sample 3 with a 1.5 nm width barrier. This value is close to the nominal thickness used in standard MTJs.

The cross-sectional specimens for TEM studies were cut along MgO(100) planes. They were glued face to face and thinned using tripod polishing[31] and ion milling at low angle and low voltage[32] to the electron transparency. The structures of the different layers and interfaces were investigated by TEM in high-resolution mode (HRTEM) using a TEM- scanning transmission electron microscope (STEM), a Tecnai F20 fitted with an objective lens corrected for spherical aberration (CEOS). Spatially resolved EELS experiments have been carried out on the same cross sections using two different microscopes. A dedicated STEM VG HB501UX operated at 100 kV equipped with a Nion aberration corrector and a Gatan Enfina EEL (probe size of 0.13 nm), and the TEM-STEM Tecnai microscope operated at 200 kV equipped with a Tridiem EEL filter (the microscope was used in its STEM mode with a probe size of 0.8 nm). EELS line spectra have been generally acquired over a 500 eV energy range including the oxygen K edge at 532 eV and the iron L edge at 708 eV.

To avoid artifactual contributions from the TEM sample preparation, from the irradiation of the sample under the beam and from energy and spatial drifts, we have worked under the following conditions: (i) Samples were cleaned by plasma cleaner prior to any analysis, (ii) EELS experiments were performed far from the edges of the sample to minimize the contribution of any possible surface oxidation, (iii) a recording time of 0.1 s per pixel for the O and Fe edges was
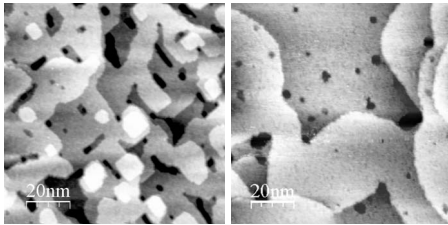
FIG. 1. STM images of the bottom Fe electrode performed before growing the MgO barrier. The image on the left side corresponds to an annealing temperature which does not exceed 700 K. The image on the right side corresponds to an annealing performed above 750 K.

used in the case of the smaller probe size (0.13 nm) to avoid irradiation damages. STEM and HREM image intensities have been recorded before and after the EELS measurements to validate the data. (iv) Sample spatial drift was controlled *in situ* during the STEM-EELS experiments using the DIGITAL MICROGRAPH acquisition software. (v) We used short recording times to minimize the energy drift, and we performed several analyses to get statistically reliable results. It should be noted that the treatment of the drift is a key experimental point because any drift during an experiment may lead to misleading interpretations.

III. EXPERIMENTAL RESULTS

A. Scanning tunneling microscopy

Typical STM images of the first Fe electrode are shown in Fig. 1. Depending on the annealing temperature, two kinds of morphology are observed. For limited annealing below 700 K, regular steps are observed aligned along [110] bcc Fe crystallographic directions. The terrace sizes are rather small, around 10 nm, and the root-mean-square (RMS) roughness is around 0.25 nm for a 200×200 nm^2 area. For higher annealing temperature, the terrace size is greatly increased to about 100 nm, but the steps are no longer straight along the [110] bcc directions. They are now curved and often link two threading dislocations. The RMS roughness is decreased to 0.12 nm for an area of 200×200 nm^2. Another important point is that regularly distributed holes are observed on the Fe surface. The higher the annealing temperature is, the higher the number and the size of the holes are. These holes are due to the dewetting of the Fe layer on MgO, since the equilibrium situation when growing Fe on MgO is three-dimensional (3D) islanding. The annealing temperature and duration have consequently to be adjusted in order to obtain wide terraces but with a limited number of holes. For this purpose, the annealing process was fixed at 750 K for 15 min.

B. HRTEM experiments

The regularity of all the stacks and the continuity of the MgO barrier have been investigated by TEM. HRTEM observations were carried out to identify the structure of the MgO barrier and the quality of the metal-oxide interfaces. Figure 2 shows the structure of the Fe/MgO/Fe MTJ with a
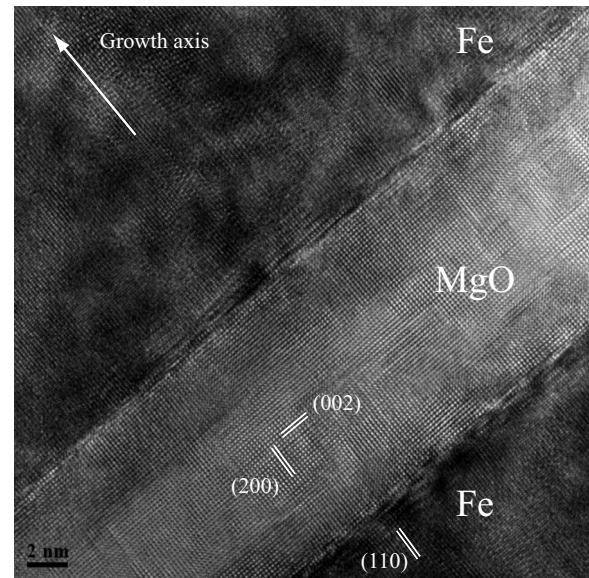
FIG. 2. HREM image of the Fe/MgO/Fe epitaxial MTJ grown on MgO with a 10 nm thick MgO barrier (sample 2).

10 nm thick MgO insulating barrier (sample 2). In the Fe layers only the (110) Fe planes (d_{110}=0.202 nm) are resolved. In the MgO barrier, both the (200) and (002) MgO planes, with an interplanar spacing of 0.21 nm in the bulk, are observed. The Fe/MgO/Fe stacking is epitaxial with the orientation relationship: Fe(001)[110]‖MgO(001)[100]. The cubic structure of bcc Fe is rotated in the interface plane by 45° with respect to that of fcc MgO. Darker areas are visible on the different samples on each side of the two Fe/MgO interfaces. These darker areas correspond to the position of the misfit dislocations. A set of diffuse and discontinuous fringes parallel to the Fe/MgO interfaces is also observed on each side of the MgO barrier. These contrasts are due to translational moiré fringes induced by interference between the (002)-type beams of Fe overlapping the (002)-type beams of MgO. This overlapping comes from the interface roughness which is responsible for a double diffraction phenomenon along the beam path. Mean value of the experimental distance between the moiré fringes is $d_M \sim 0.48$ nm ± 0.02 nm, in good agreement with the theoretical value given by the relation $d_M = d(\text{Fe})_{(002)} d(\text{MgO})_{(002)} / [d(\text{Fe})_{(002)} - d(\text{MgO})_{(002)}]$=0.47 nm [calculated with $d(\text{Fe})_{(002)}$=0.14 nm and $d(\text{MgO})_{(002)}$=0.2 nm].

Additional phases cannot be detected at the Fe/MgO interfaces. The contrast due to misfit dislocations and moiré fringes prevents any conclusion on the formation of very thin iron oxide layers. Moreover, the Fe-O distances which are expected at the interface only differ by 0.015 nm between an oxidized and a nonoxidized interface.[25,33]

C. EELS experiments

EELS line spectra, i.e., sequences of EELS spectra measured for successive positions of the subnanometer probe on the specimen,[34] can be recorded in different directions. The Fe and MgO layers can be clearly identified by monitoring
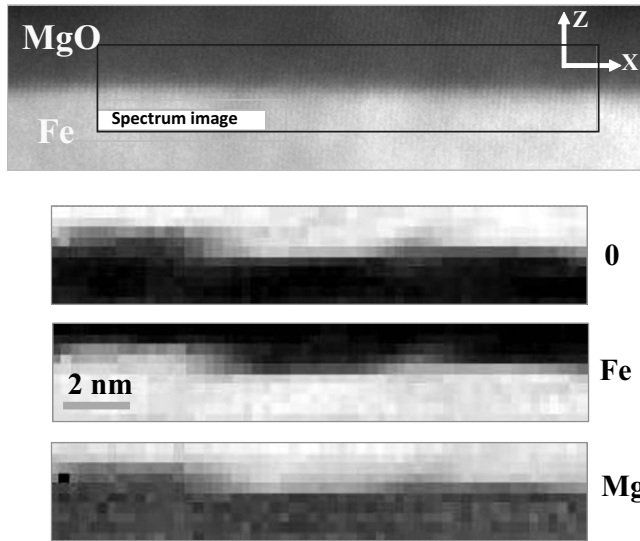
FIG. 3. (a) Annular dark field image (ADF) of the bottom Fe/MgO interface in sample 1 using the lowest probe size available (0.13 nm) and corresponding O, Fe, and Mg chemical maps. The spectrum image has been treated by principal component analysis (Refs. 35).

the oxygen K edge (at 532 eV) and the iron $L_{2,3}$ edge (at 710 eV) as functions of the probe position. These edges are further used to measure the local oxygen and iron contents. Line spectra recorded in directions parallel and perpendicular to an interface provide quantitative data on the characteristic width and height of the roughness, averaged over the thickness of the sample. Changes in the energy-loss near-edge structures allow the identification of the extent of Fe-O bonds formed at the interfaces.

The first series of EELS experiments has been performed on sample 1 to analyze the bottom Fe/MgO interface (Figs. 3 and 4). A very small probe size (0.13 nm) and a pixel step of 0.3 nm have been used to record the oxygen K, iron L edge, and magnesium K profiles along the Fe/MgO interface. The corresponding composition variations are shown in Figs. 3 and 4, in which the z direction corresponds to the growth axis and the x direction is parallel to the interface. Spectra have been recorded along ten lines parallel to the interface, and principal component analysis (PCA) has been applied to reduce the noise.[35] Figure 3 displays the two-dimensional (2D) elemental cartography. The Mg and O chemical maps are nicely correlated, while the O and Fe chemical maps are evidently anticorrelated. The variations of the Fe, O, and Mg composition are due to the presence of steps, which are clearly visualized in the elemental maps. The specimen thickness was about 40 nm and from the STM image of Fig. 1 it can be seen that we expect either zero or one atomic step within the specimen thickness from the as-deposited roughness level. To measure the extent of the roughness after deposition of the MgO layer in the growth direction and perpendicularly, the 3D chemical composition has plotted in Fig. 4. The vertical arrow shows a small area at the interface which corresponds to a minimum of the Fe concentration and to a maximum of the oxygen concentration. This area contains two Fe steps separated by a MgO terrace extended over
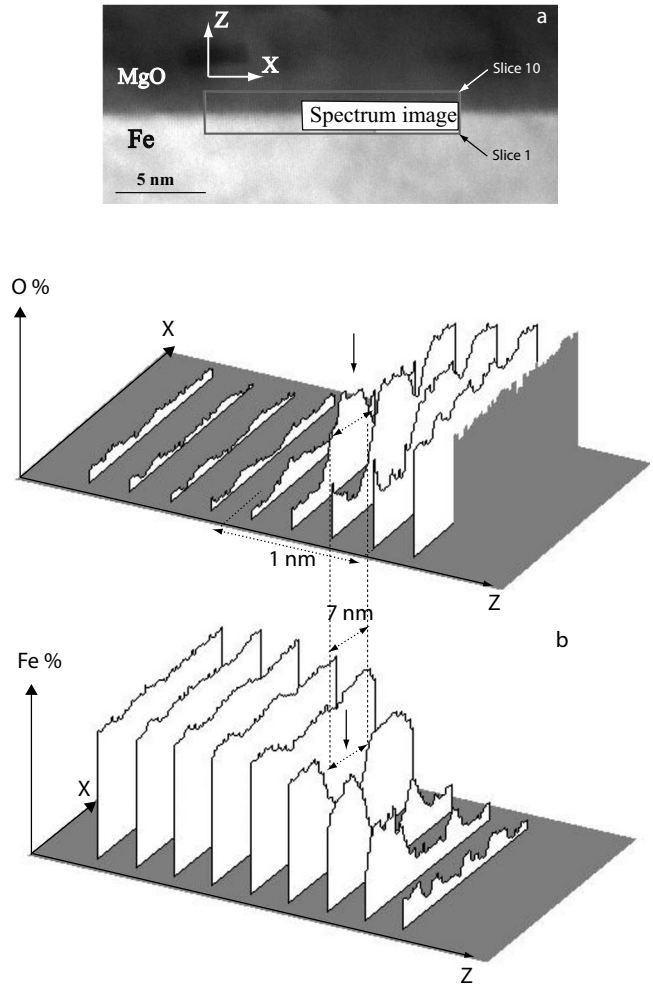
FIG. 4. (a) ADF of the bottom Fe/MgO interface in sample 1 using the lowest probe size available (0.13 nm). (b) O and Fe concentrations along the x and z axes measured from the spectrum image which contains ten slices [see window in Fig. 4(a)]. Vertical arrows show an area with a maximum of O concentration and a minimum of Fe concentration. The spectrum image has been treated by principal component analysis (Ref. 35).

~7 nm, the same size as a typical hole seen in the STM image. The spatial variations of the Fe and O concentrations are complementary. The interpenetration of the Fe and MgO phases is a consequence of the interface roughness. These results show that the RMS roughness measured by STM on the free Fe surface is preserved after the growth of the MgO layer.

The second series of EELS experiments has been performed with the FEI Tecnai F20 electron microscope using a probe size of 0.8 nm and a pixel step of 0.5 nm. The analysis has been performed along the growth axis of sample 2 and the two Fe/MgO and MgO/Fe interfaces have been investigated. Figure 5(a) displays the bright field STEM image of the sample, on which the oxygen and iron composition profiles have been superimposed. The spatial variations of the O and Fe contents look similar at the Fe/MgO and MgO/Fe interfaces. In Fig. 5(b) the concentration profiles at the two interfaces have been superimposed (mirrored with respect to the x-y plane for the bottom interface). In the range of
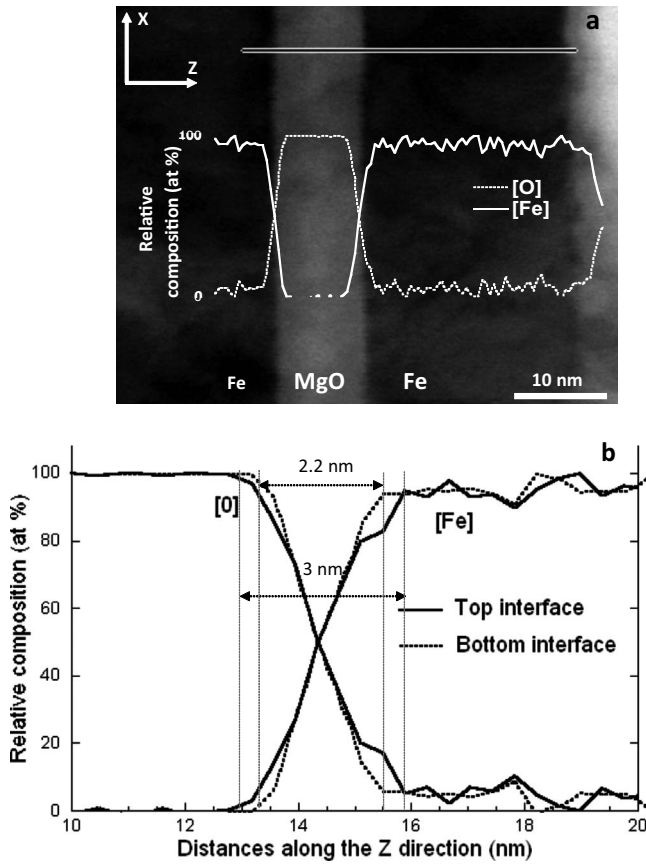
FIG. 5. (a) Bright field STEM image of sample 2. Gray line indicates the position of the EELS line scan; the associated variation of [Fe] and [O], obtained after PCA analysis, is superimposed. (b) Fe and O contents near the top interface superimposed with those near the bottom interface. For clarity, the curves related to the bottom interface have been mirrored.

20–80 at % the slope of the chemical concentration behaves similarly for the two interfaces. However when we look at the 0%–100% width of the signals we find that the upper interface appears to 0.8 nm broader, as shown in Fig. 5(b). This suggests that there may be some additional roughness or interdiffusion at the upper interface. We will see below that the fine-structure analysis confirms this hypothesis. The difference between the extent of the bottom interface measured in Figs. 4 and 5(b) can be explained by a different beam broadening or by the probe size convolution.

The fine structures in the EELS spectra convey a signature of the coordination and bonding state of the relevant atoms, for instance of a possible hybridization between Fe and O at each interface. Spectra extracted from the line scan shown in Fig. 5 are displayed in Fig. 6, together with reference spectra for iron oxide and iron metal. The oxygen K edge fine structure recorded at the top interface presents a small shoulder at 531 eV. This satellite peak coincides with the energy of the first peak in the iron oxide spectrum. While this peak may correspond to traces of Fe-O hybridization, its low intensity does not allow us to make firm conclusions on differences between the two interfaces. Figure 6 also displays the iron $L_{2,3}$ edge fine structure. The background has been removed using the same conditions for all the spectra.
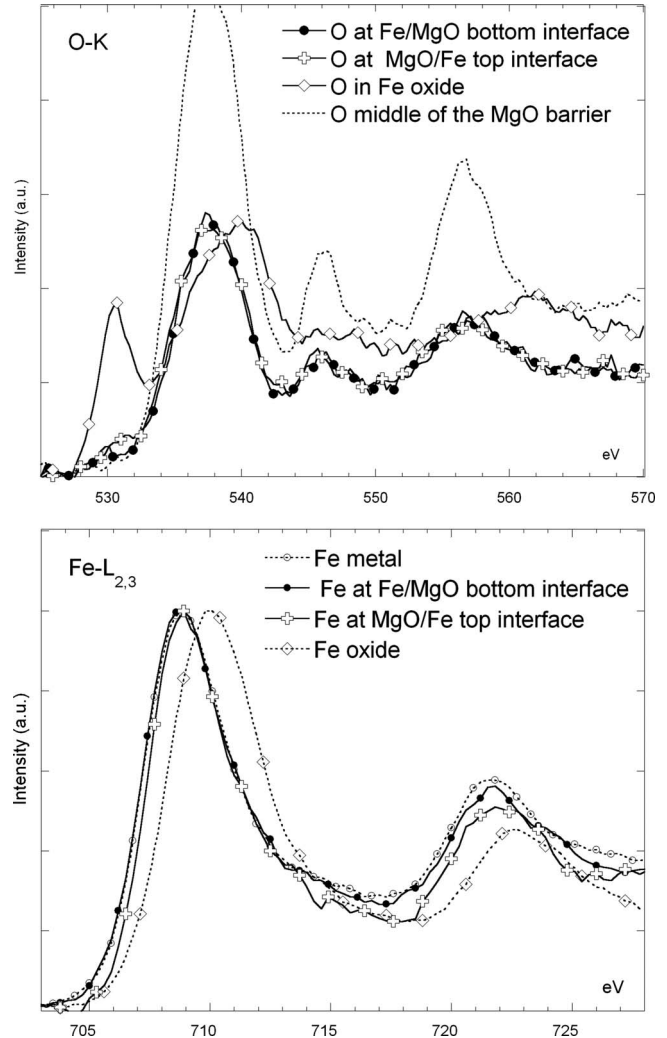
FIG. 6. O and Fe spectra extracted from the line spectrum presented in Fig. 5 at the two positions where the Fe and O concentrations are identical. The Fe metal reference is taken far from the interface. The Fe oxide reference spectrum corresponds to the edge of the sample.

The spectrum at the bottom interface is close to that of metallic iron, while the fine structure slightly changes at the top interface where the ratio $I(L_3)/I(L_2)$ seems to increase and becomes closer to the value measured in the reference oxide. This trend is confirmed by quantitative measurements of the white line ratio from the second derivative signal[36,37] of the spectrum line reconstructed by PCA. Figure 7 displays this result. The slight difference between the Fe-$L_{2,3}$ energy loss near edge structure (ELNES) suggests that a larger overlapping of the MgO and Fe terraces exists at the top interface. Fe atoms have more bonds with O atoms at the top interface and this can be explained by the different extent of the roughness. At the energy resolution used to record simultaneously the O and Fe (required here), the chemical shifts of the Fe $L_{2,3}$ edge and the O prepeak intensity are not reliably extracted. This confirms that the hybridization is relatively weak, consistent with the small amount of intermixing seen in the line traces of Fig. 5.

Figure 8 shows the spatial variations of the O and Fe contents measured with a probe size of 0.13 nm along the
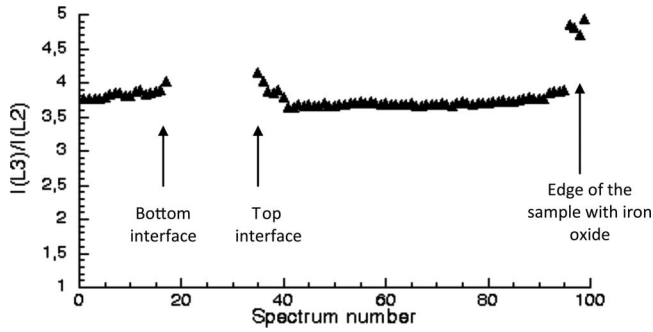
growth axis of a MTJ with a 1.5 nm thick MgO barrier. The iron EELS signal does not vanish when the probe is located at the center of the barrier at about ~1 nm from the interface position measured by the HREM measurements. This does not necessarily mean that some Fe/MgO interdiffusion occurs, but it can simply be explained by broadening of the beam due to dechanneling.
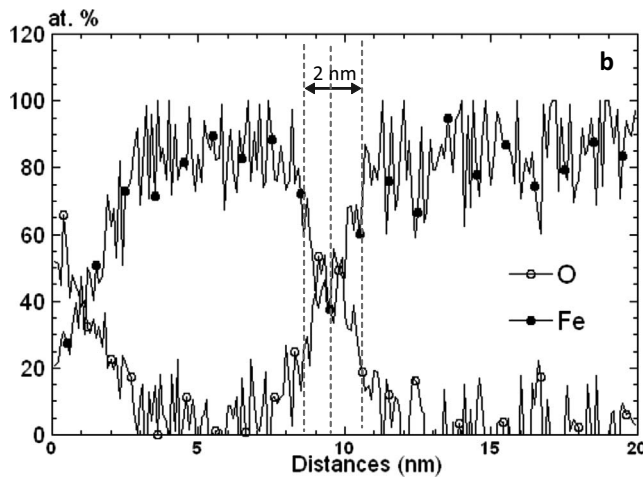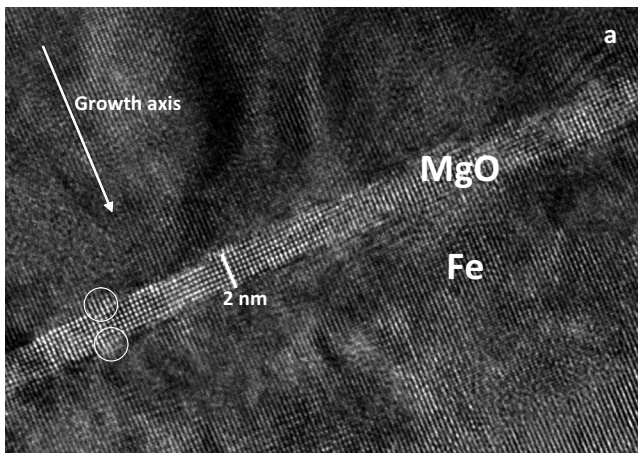
FIG. 8. (a) HREM image of sample 3. (b) Variations of the Fe and O concentrations across the junction for the sample 3 (nominal value of MgO barrier: 1.5 nm). The width of the barrier measured by HREM is shown for guide line and its irregularity is highlighted by white circles.
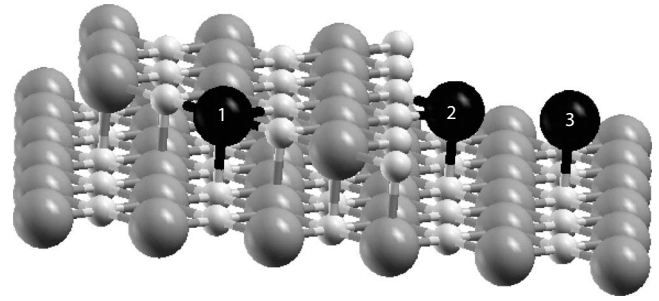
FIG. 9. This figure shows an iron atom located at the edge of a flat (001) MgO island. The Fe atoms located at the (010) and (110) edges of the island are, respectively, fourfold (position 1) and threefold (position 2) coordinated. As a matter of comparison, a single-coordinated Fe atom located on the top of the flat substrate (position 3) is also shown in the figure.

IV. DISCUSSION AND CONCLUSION

The present paper intends to provide an insight at the atomic level onto the structural and chemical properties of the metal-insulator interfaces involved in a magnetic tunnel junction. It therefore complements the information provided by well-established techniques: XPS and XAS, which probe the response averaged over wide areas and STM which is a local approach with atomic resolution but which applies to free surfaces accessible at different stages of the growth process. STM observations are therefore not useful to investigate the buried interfaces involved in the device.

Transmission electron microscopy studies on cross section are well adapted for a local investigation. However, high-resolution images are generally not capable of providing unambiguous information. They exhibit intensities which are governed by many factors when the composition varies along the beam trajectory. The reported moiré fringes constitute one of these puzzling effects.

Emphasis has therefore being put in this work on the use of the characteristic EELS signals, recorded in a spatially resolved mode, i.e., when scanning a minute probe of electrons over the specific area of interest. At the level of resolution achieved here, this constitutes a first demonstration. It clearly reveals the existence of atomically thick terraces, and not of a composition gradient with diffusion of species, at the interfaces. Widths and heights have been imaged and measured. A weak asymmetry between the bottom and top interfaces (following the growth direction of the device) has been identified through the increase of the terrace thickness visible in chemical maps with atomic resolution and the existence of a feature indicating formation of some Fe-O bonds on the top interface. For this second interface, hybridization may be considered as a consequence of the roughness. Figure 9 proposed possible environments of the Fe atoms at a step: a flat (001) MgO island grown on a (001) MgO substrate. This type of islands has been found energetically favorable and has already been observed.[38] The Fe atoms located at the [010] and [110] edges are, respectively, fourfold and threefold coordinated. As a matter of comparison, a single-coordinated Fe atom located on the top of the flat substrate is also shown in the figure. Locally, the environment of the Fe

atoms is thus O rich at the interface onset and the amount of Fe-O interaction will depend on the extent and size of the MgO islands. This behavior is strongly dependent on the synthesis processes and in particular on intermediate annealing treatments, only possible for the bottom electrode, to reduce the roughness.

These results constitute clear hints for the understanding of the measured transport properties in these MTJs, since the structural and chemical asymmetries of the junction may be related to the asymmetry observed in the bias-dependent conductance and TMR, as reported by several groups.[10,18] Such an influence of the atomic and chemical structures on the magnetotransport behavior has recently been confirmed by *ab initio* calculations of tunnel conductivity of Fe/MgO/Fe MTJs and Fe/Fe-O/MgO JTMs.[39]

*Corresponding author. FAX: +33-5-62-25-79-99; serin@cemes.fr

[1] J. S. Moodera, Lisa R. Kinder, Terrilyn M. Wong, and R. Meservey, Phys. Rev. Lett. **74**, 3273 (1995).

[2] S. S. Parkin, K. P. Roche, M. G. Samant, P. M. Rice, and R. B. Beyers, J. Appl. Phys. **85**, 5828 (1999).

[3] J. J. Sun, V. Soares, and P. P. Freitas, Appl. Phys. Lett. **74**, 448 (1999).

[4] J. Wang, P. P. Freitas, and E. Snoeck, Appl. Phys. Lett. **79**, 4553 (2001).

[5] C. Tiusan, T. Dimopoulos, K. Ounadjela, M. Hehn, H. A. M. van den Berg, V. da Costa, and Y. Henry, Phys. Rev. B **61**, 580 (2000).

[6] L. Le Brizoual, M. Hehn, E. Snoeck, F. Montaigne, M. Alnot, A. Schuhl, and P. Alnot, Appl. Phys. Lett. **86**, 112505 (2005).

[7] D. J. Smith, M. R. McCartney, C. L. Platt, and A. E. Berkowitz, J. Appl. Phys. **83**, 5154 (1998).

[8] J. Mathon and A. Umerski, Phys. Rev. B **63**, 220403(R) (2001).

[9] W. H. Butler, X.-G. Zhang, T. C. Schulthess, and J. M. MacLaren, Phys. Rev. B **63**, 054416 (2001).

[10] S. Yuasa, T. Nagahama, A. Fukushima, Y. Suzuki, and K. Ando, Nature Mater. **3**, 868 (2004).

[11] M. Sicot, Ph.D. thesis, University H. Poincaré-Nancy I, 2005.

[12] R. Guerrero, D. Herranz, F. G. Aliev, F. Greullet, C. Tiusan, M. Hehn, and F. Montaigne, Appl. Phys. Lett. **91**, 132504 (2007).

[13] S. Yuasa, A. Fukushima, H. Kubota, Y. Suzuki, and K. Ando, Appl. Phys. Lett. **89**, 042505 (2006).

[14] S. S. P. Parkin, C. Kaiser, A. Panchula, P. M. Rice, B. Hughes, M. Samant, and S.-H. Yang, Nature Mater. **3**, 862 (2004).

[15] J. Hayakawa, S. Ikeda, Y. M. Lee, F. Matsukura, and H. Ohno, Appl. Phys. Lett. **89**, 232510 (2006).

[16] F. Greullet, C. Tiusan, F. Montaigne, M. Hehn, D. Halley, O. Bengone, M. Bowen, and W. Weber, Phys. Rev. Lett. **99**, 187202 (2007).

[17] C. Tiusan, J. Faure-Vincent, C. Bellouard, M. Hehn, E. Jouguelet, and A. Schuhl, Phys. Rev. Lett. **93**, 106602 (2004).

[18] C. Tiusan, M. Hehn, F. Montaigne, F. Greullet, S. Andrieu, and A. Schuhl, J. Phys.: Condens. Matter **19**, 165201 (2007).

[19] O. Wunnicke, N. Papanikolaou, R. Zeller, P. H. Dederichs, V. Drchal, and J. Kudrnovsky, Phys. Rev. B **65**, 064425 (2002).

[20] X.-G. Zhang, W. H. Butler, and A. Bandyopadhyay, Phys. Rev. B **68**, 092402 (2003).

[21] M. Sicot, S. Andrieu, P. Turban, Y. Fagot-Révurat, H. Cercellier, A. Tagliaferri, C. De Nadai, N. B. Brookes, F. Bertran, and F. Fortuna, Phys. Rev. B **68**, 184406 (2003).

[22] M. Sicot, S. Andrieu, F. Bertran, and F. Fortuna, Phys. Rev. B **72**, 144414 (2005).

[23] E. Popova, J. Faure-Vincent, C. Tiusan, C. Bellouard, H. Fischer, E. Snoeck, M. Hehn, F. Montaigne, M. Alnot, S. Andrieu, and A. Schuhl, Appl. Phys. Lett. **81**, 1035 (2002).

[24] P. Luches, S. Benedetti, M. Liberati, F. Boscherini, I. I. Pronin, and S. Valeri, Surf. Sci. **583**, 191 (2005).

[25] H. L. Meyerheim, R. Popescu, N. Jedrecy, M. Vedpathak, M. Sauvage-Simkin, R. Pinchaux, B. Heinrich, and J. Kirschner, Phys. Rev. B **65**, 144433 (2002).

[26] L. Samet, D. Imhoff, J.-L. Maurice, J.-P. Contour, A. Gloter, T. Manoubi, A. Fert, and C. Colliex, Eur. Phys. J. B **34**, 179 (2003).

[27] A. Falqui, V. Serin, L. Calmels, E. Snoeck, A. Corrias, and G. Ennas, J. Microsc. **210**, 80 (2003).

[28] D. M. Muller, L. Fitting Kourkoutis, M. Murfitt, J. H. Song, H. Y. Hwang, J. Silcox, N. Dellby, and O. Krivanek, Science **319**, 1073 (2008).

[29] P. Turban, L. Hennet, and S. Andrieu, Surf. Sci. **446**, 241 (2000).

[30] J. Faure-Vincent, C. Tiusan, E. Jouguelet, F. Canet, M. Sajieddine, C. Bellouard, E. Popova, M. Hehn, F. Montaigne, and A. Schuhl, Appl. Phys. Lett. **82**, 4507 (2003) and references herein.

[31] M. R. Brickey and J. L. Lee, Microsc. Microanal. **6**, 231 (2000).

[32] A. Barna, *Topographic Kinetics and Practice of Low Angle Ion Beam Thinning, Workshop on Specimen Preparation for TEM of Materials III*, edited by R. Anderson, Materials Research Symposium Proceedings **254**, 3–22 (Materials Research Society, Pittsburg, 1992).

[33] C. Wang, S. G. Wang, A. Kohn, Roger C. C. Ward, and A. K. Petford-Long, IEEE Trans. Magn. **43**, 2779 (2007).

[34] M. Tencé, M. Quartuccio and C. Colliex, Ultramicroscopy **58**, 42 (1995).

[35] N. Bonnet and D. Nuzillard, Ultramicroscopy **102**, 327 (2005).

[36] G. A. Botton, C. C. Appel, A. Horsewell, and W. M. Stobbs, J. Microsc. **180**, 211 (1995).

[37] F. W. Lytle, G. van der Laan, R. B. Greegor, E. M. Larson, C. E. Violet, and J. Wong, Phys. Rev. B **41**, 8955 (1990).

[38] G. Geneste, Ph.D. thesis, University Toulouse III, 2003.

[39] X.-G. Zhang, W. H. Butler, and A. Bandyopadhyay, Phys. Rev. B **68**, 092402 (2003); M. Chshiev, private communication.